ELSEVIER SAUNDERS

POSITRON EMISSION TOMOGRAPHY

PET Clin 2 (2007) 161–172

Clinical and Research Applications of Quantitative PET Imaging

Sandip Basu, MD[a], Habib Zaidi, PhD, PD[b], Abass Alavi, MD[a,*]

Positron emission tomography (PET) with ^{18}F-Fluorodeoxyglucose (FDG) was introduced as a research tool and a quantitative method for calculation of absolute glucose metabolic rate in an area of interest [1,2]. These initial quantitative approaches, although reliable, were technically demanding and required arterial blood sampling at multiple time points and complex mathematical operations. However, with the recent rapid increase in the number of clinical applications of FDG-PET, the quantitative kinetic modeling approach was found to be impractical for routine clinical use. Efforts were made to develop quantitative methods that would be simple yet reasonably accurate and that could complement visual image interpretation and minimize the interobserver variability that is commonly encountered [3]. Some of the recent developments in quantitative PET imaging will be reviewed in this article, which will emphasize certain technical issues related to this powerful methodology.

The various methods of PET data analysis can be primarily classified into three major groups: (1) qualitative analysis or visual assessment,

[a] Department of Radiology, Division of Nuclear Medicine, Hospital of the University of Pennsylvania, 3400 Spruce Street, Philadelphia, PA 19104-4283, USA
[b] Division of Nuclear Medicine, Geneva University Hospital, CH-1211 Geneva, Switzerland
* Corresponding author. Department of Radiology, Division of Nuclear Medicine, Hospital of the University of Pennsylvania, 3400 Spruce Street, 1 Donner Building, Philadelphia, PA 19104-4283.
E-mail address: abass.alavi@uphs.upenn.edu (A. Alavi).

1556-8598/07/$ – see front matter
doi:10.1016/j.cpet.2007.10.002
pet.theclinics.com

(2) semi-quantitative analysis, which includes standardized uptake value (SUV) and lesion-to-background ratio (L:B ratio), and (3) absolute quantitative analysis, including (a) nonlinear regression (NLR), (b) Patlak graphical analysis and derived methods, and (c) simplified quantitative methods. Among these, the approaches in the first two categories (ie, the visual assessment, SUV and L:B ratio) and the simplified quantitative methods of the last category are relatively easy to employ in clinical settings, while the absolute quantitative measurements generated by dynamic imaging and blood sampling have been generally reserved for research applications.

Advantages of quantitative FDG-PET compared with qualitative visual assessment

Visual assessment of the PET images forms the basis of the interpretation of any PET study in the daily practice of this modality. An abnormal focus of FDG uptake in a pathological lesion is the result of "metabolic contrast" in the abnormal sites compared with the surrounding background. This contrast is a function of three principal factors: (1) the concentration of glucose transporter expression in the cell surface, (2) hexokinase activity, and (3) the level of glucose-6-phosphatase in the cell. The major concern with regard to visual assessment has been the subjective nature of the assessment of contrast and thus the significant inter- and intraobserver variability of PET image interpretation. This has important implications for clinical trials where objective assessments are essential. No clear-cut widely accepted criteria have been established to reduce this subjectivity among PET readers. This has led to endeavors to define an objective quantitative technique that would be practical and at the same time reasonably accurate.

Quantitative methods for absolute assessment of glucose metabolic rate

Quantitative metabolic rate assessment by kinetic modeling can measure FDG metabolism and also yield individual rate constants and thereby provide insight into the various components of glucose metabolism such as transport and phosphorylation. Compartmental modeling describes the behavior of FDG in cells mathematically and was developed to describe the kinetics of the glucose analogs [^{14}C]-deoxyglucose and FDG in the pioneering work on tracer kinetic modeling [1,2,4–6]. The tracer kinetic modeling of FDG is based on a standard three-compartment kinetic model (Fig. 1), with two tissue compartments and a single arterial input function. Compartment 1 (C_1) represents the arterial concentration of free FDG in plasma. The first tissue

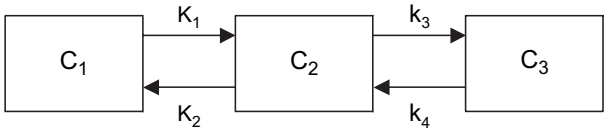

Fig. 1. Three-compartment kinetic model of FDG behavior. C_1 is concentration of unmetabolized activity in arterial plasma, C_2 is concentration of free tracer in tissue, and C_3 is concentration of tracer after phosphorylation.

compartment (C_2) represents an extravascular pool of tracer in the tissue, which is available for phosphorylation, and the final compartment (C_3) is the concentration of FDG that has undergone phosphorylation by hexokinase. Dynamic scanning data coupled with rapid arterial blood sampling provide time-activity curves for the specific tumor, organ, or tissue under study. Using nonlinear least squares approximations, these curves can be fit to obtain the various rate constants. Dephosphorylation of FDG-6-phosphate is generally ignored, although more accurate kinetic modeling, which includes this reverse process, can lead to accurate results.

The glucose metabolic rate (MRglu) is calculated by the following equation:

$$\text{MRglu} = \frac{C_p}{LC} \times \frac{K_1 \cdot k_3}{k_2 + k_3} = \frac{C_p}{LC} \times K_i \qquad (1)$$

where C_p = plasma glucose concentration, K_1, k_2 = rate constants for forward and reverse transport of FDG, respectively, k_3 = rate of phosphorylation of FDG, K_i = net rate of influx of FDG, and LC = lumped constant relating FDG kinetics to that of glucose. Errors in accurately assessing MRglu, or K_i, include the variance and covariance of the rate constants extracted from the fitting procedure (dependent on the noise in the imaging data), partial volume effects, inaccurate assumptions underlying the model (such as a zero value for k_4), and the contribution from blood pool activity in the imaging data. Initially described in brain imaging [7,8], these were extrapolated into tumor imaging as well. The methods described are nonlinear regression, Patlak graphical analysis, and Patlak-derived methods [9]. These methods (except for the simplified quantitative techniques) all involve dynamic scanning.

The general advantages of dynamic quantitative approaches include the availability of dynamic data and a low dependency on imaging time; however, there are certain disadvantages of dynamic quantitative approaches. They are complex, technically demanding and time-consuming procedures; they require a dynamic scanning protocol; and there is a need for arterial blood sampling (unless heart is in the field of view of the scanner) or dynamic imaging of a blood-pool structure to obtain a precise input function [9]. In addition,

dynamic scanning is a disadvantage in cancer patients with multiple lesions scattered throughout the body. The field of view of the study in dynamic imaging methods like NLR or Patlak-Gjedde analysis is limited to one bed position. Hence, lesions in the specific bed position can be assessed but additional scans are required to assess the other lesions.

Nonlinear regression analysis

In this method, the net rate of FDG influx (K_i) is estimated from dynamic PET data and from a standard two-tissue compartment model, arterial input function, and NLR analysis [6]. The advantages of this technique are that it is quantitative, independent of uptake period, and provides insight into various rate constants. The usual disadvantages of a dynamic study make its implementation complex.

Patlak–Gjedde graphical analysis

In this technique, originally described by Patlak and colleagues [8], the regional concentration at time t after injection can be obtained by the following equation:

$$c(t) = \lambda \cdot c_p(t) + K_i \int_0^T c_p(t)\, dt \qquad (2)$$

where $c(t)$ = activity in the tissue as measured by the PET scanner at time t, $c_p(t)$ = concentration of FDG in the plasma, $\lambda >$ = partition coefficient of FDG, K_i = net rate of FDG influx into the tissue, and T = duration of the PET scan.

This technique has the following advantages: it is more robust compared with NLR method; compared with NLR analysis it uses a simplified scanning protocol, lacks noise amplification, and can generate parametric images. However it has the disadvantages of dynamic scanning, and compared with NLR analysis, individual rate constants like K_1 and K_3 cannot be obtained.

Simplified kinetic method

Originally described by Hunter and colleagues [10], this method requires only a static scan and a few (venous) blood samples during the scan. These samples are then used to scale a population-derived average plasma curve. This method is able to estimate glucose metabolism without the need for a dynamic scan and with a substantially reduced blood sampling protocol. Compared to the SUV method, it takes into account changes in plasma clearance. A potential drawback of this method is that the correction for differences in plasma clearance is only a first-order correction (the peak is assumed to be constant). This method needs to be validated in a large patient population.

Standardized uptake value method: potentials and pitfalls and the recent concepts

SUV (synonyms used in literature: differential absorption ratio [DAR], differential uptake ratio [DUR], or standardized uptake ratio [SUR]) is the most popular semiquantitative index in the clinical PET centers across the world. It provides a semiquantitative measure of FDG metabolism and is defined as the tissue concentration of tracer, as measured by PET, divided by the injected dose normalized to patient weight multiplied by a decay factor [11].

It is calculated by dividing the activity concentration in the region of interest (ROI) drawn around the lesion (MBq/mL) by the injected dose (MBq) divided by the body weight (g):

$$SUV = \frac{Mean\ ROI\ concentration\ (MBq/ml)}{Injected\ dose\ (MBq)/Body\ weight(g)} \times \frac{1}{decay\ factor\ of\ ^{18}F} \qquad (3)$$

Advantages and shortcomings of simple standardized uptake value measurement and variables affecting standardized uptake value

SUV estimation is usually an automated procedure and can be readily calculated with current software supplied with commercial PET scanners. There exists a linear relationship between the SUV and the rate of glucose metabolism as measured by kinetic modeling. Two studies [12,13] have documented this and registered correlation coefficients of 0.91 and 0.84, respectively. The correlation improves further when body surface area or lean body mass is used for normalization rather than body weight .The SUV method is technically less demanding and computationally simple (with no requirement for blood sampling) and requires considerably less scanner time than the dynamic acquisition protocols. As a result, this method has replaced the more cumbersome dynamic procedures in routine clinical practice for assessing metabolism in the tumors and other diseases.

Factors affecting the reliability of standardized uptake value

Several factors can affect the reliability of SUV [14] (**Table 1**). Important among these are (1) time interval between injection and imaging, (2) degree of infiltration of administered FDG dose at the site of injection, (3) residual activity in the syringe, (4) correction for the decay of the injected dose,

Table 1: **Factors influencing SUV determination for FDG at intended regions of interest, their undesirable effects, and associated required corrective measures**

Factor	Effects	Corrective measures
	A. Patient-rRelated factors	
Body size and habitus	Overestimation of SUV in heavier subjects with higher fat content	Use of lean body mass (SUV_{LBM}) or body surface area (SUV_{BSA}) as normalization factor
Serum glucose levels	Reduced FDG uptake in target tissues with increasing blood glucose levels	Control of blood glucose before administering FDG and applying correction factor for glucose level
	B. Technical factors	
Duration of uptake period	Increase in SUV with increasing time in malignant lesions after injection	Standardize initiation of image acquisition following administration of FDG
Partial-volume effects	Underestimation of SUV in lesions with diameters that are smaller than 2 to 3 times the spatial resolution of the scanner	Adopt an optimal partial volume correction factor
Size of the ROI and non uniformity of tracer distribution in the lesion	Low SUV_{mean} for large ROIs and high random errors in smaller ROIs	Standard size ROIs placed reproducibly in the same location, SUV_{max} preferable to SUV_{mean}.
Attenuation correction and reconstruction methods (spatial filter kernel, image resolution, number of iterations)	Underestimation of SUV with highly smooth reconstruction	Standardize acquisition and reconstruction algorithms for optimal comparison among serial imaging sessions.

Abbreviations: FDG, ^{18}F-Fluorodeoxyglucose; ROI, region of interest; SUV, standardized uptake value.
From Basu S, Zaidi H, Houseni M, et al. Novel quantitative techniques for assessing regional and global function and structure based on modern imaging modalities: implications for normal variation, aging and diseased states. Sem Nucl Med 2007;37:223–39.

and (5) partial volume effects because of limited spatial resolution of the PET instrument.

Standardized uptake value dependence on body habitus

In most current generation PET scanners, the SUV is normalized to patient body weight (designated as SUV_{BW}). However, body habitus may also be important, since adipose tissue typically demonstrates lower FDG uptake compared with other tissues owing to much less metabolic activity. Consequently, in heavier patients with a high fraction of total body fat, SUV is overestimated in non-adipose tissues. Studies have investigated the feasibility of correcting SUV with regard to other parameters such as lean body mass (SUV_{LBM}) and body surface area (SUV_{BSA}) and found them to be superior [15–17] compared with SUV_{BW}. The latter corrective methods reduce the variation of SUV related to the patient body composition and habitus.

Kim and colleagues [15] examined the value of normalization of SUV with body surface area (SUV_{BSA}) in 44 patients with cancer with body weights ranging from of 45 to 115 kg. They observed a strong positive correlation between SUV_{BW} and body weight but only a weak correlation between SUV_{BSA} and body weight with a near flat regression line. These authors concluded that SUV_{BW} overestimates FDG uptake in large patients and that SUV_{BSA} is preferable to SUV_{BW}. Subsequently two studies have confirmed this observation, and have concluded that SUV_{BSA} was superior to both SUV_{BW} and SUV_{LBM}. Zasadny and Wahl [18] addressed the same concern by studying the relationship between SUVs in normal tissues and body weight in 28 nondiabetic women with newly diagnosed untreated primary breast cancer with body weights ranging from 45 to 107 kg, and observed a positive correlation between SUV and body weight for liver and spleen metabolic activity. In heavy patients, SUVs for these tissues were up to two times higher than those of the lighter patients. They concluded that correction of SUV for lean body mass (SUV_{LBM}) eliminated the weight dependence of the SUV. Nevertheless, some authors feel that these differences between the normalization methods are small except in very obese patients [19].

Standardized uptake value dependence on blood glucose level

Several studies have demonstrated that SUVs of malignant lesions depend substantially upon glycemic status. Also, hyperinsulinemia leads to enhanced glycolysis in adipose tissue and in muscles, and thereby results in low SUV values in other tissues. Most PET centers usually require a maximum plasma glucose level ranging from 150 to 200 mg/dL in patients undergoing FDG-PET studies. Interestingly, Zhuang and colleagues [20] noted that the effects of glucose concentration differ between malignant disorders and inflammatory processes. They observed that elevated blood glucose levels up to 250 mg/dL do not appear to affect the SUV in the inflammatory or other benign lesions.

Standardized uptake value changes over time, implications of dual-time point, and delayed imaging in differentiating cancer from benign diseases

Currently most centers employ SUV measurement at a single time point by assigning a standard ROI. It is clear that variations in the time interval between tracer injection and image acquisition (ie, FDG uptake period) substantially influence SUV. Hamberg and colleagues [21] demonstrated that the equilibrium time (no change in concentration of this compound) in bronchial carcinoma varied from 256 to 340 minutes postinjection, and decreased after therapy to 123 to 185 minutes postinjection. These authors concluded that the time interval of 45 to 60 minutes leads to a significant underestimation of true SUV because, in most tumors, FDG uptake continues to rise beyond this period, and typically does not reach a plateau for several hours. Lodge and colleagues [22] also noted that in high-grade sarcomas, maximal FDG uptake was at 4 hours whereas such equilibrium was achieved within 30 minutes in benign lesions. Investigators at the University of Pennsylvania, in their study of FDG uptake over extended time periods (over 8 hours) in patients with non–small-cell lung cancer showed that while tumor sites revealed increased uptake of FDG over 3 to 4 hours, surrounding normal tissues showed declining values with time. These data indicate that SUV in normal and abnormal tissues change substantially over time and therefore the time interval between the administration and imaging should be taken into consideration in such measurements.

Also, there exists considerable overlap between active inflammatory processes and malignant lesions when SUV is employed for this distinction. Therefore, a threshold value for SUV alone cannot be used to differentiate between the two. Several approaches have been explored to enhance the specificity of FDG-PET for assessing potential malignant lesions. For example, dual-time point FDG-PET imaging has been used in assessing various malignancies including those of the head and neck [23], lung [24], breast [25–27] gallbladder [28], cervix [29], and central nervous system [30]. The theoretical basis for the role of this approach in this setting lies in the fact that dephosphorylation in tumor cells is either absent or very slow compared with that in normal cells because of their low glucose-6-phosphatase content. This results in a build up of contrast between malignant lesions and the normal tissues with time, which further increases lesion detectability on delayed images. This approach has been tested by several investigators as a potential way to distinguish malignant from benign lesions.

Hustinx and colleagues [23] examined the utility of dual-time point scanning in 21 patients with head and neck cancer who were scanned serially at two time points, the first at 70 minutes (range 47 to 112) and the second at 98 minutes (range 77 to 142) after the intravenous injection of FDG. The mean interval between emission scans was 28 minutes (range 13 to 49). SUVs were generated for the cerebellum, tongue, larynx, malignant lesion, and a matched contralateral site. Tumor SUVs were 4.0 ± 1.6 (mean $\pm$ SD) for the first scan and 4.5 ± 2.2 for the second scan. Corresponding SUVs for the contralateral sites were 1.2 ± 0.5 and 1.1 ± 0.5 for the two scans, respectively. Tumor SUVs increased by $12\% \pm 12\%$ as compared with a $5\% \pm 17\%$ decrease for contralateral sites ($P < .05$). SUVs for inflammatory lesions (2.0 ± 0.7 and 2.0 ± 0.9), cerebellum (4.2 ± 1.3 and 4.3 ± 1.4), tongue (1.8 ± 0.4 and 1.9 ± 0.5), and larynx (1.5 ± 0.6 and 1.5 ± 0.6) remained constant over time ($+0.6\%$, $+2.8\%$, $+1.4\%$, and -2.4%; $P < .05$ when compared with tumor SUV changes). The ratio of tumor SUV to contralateral SUV increased by $23\% \pm 29\%$ over time whereas this ratio for inflammatory sites increased by only $5\% \pm 15\%$ ($P = .07$). They proposed this approach as a useful means for differentiating malignant lesions from inflammation and nonspecific uptake in normal tissues.

Matthies and colleagues [24] investigated this method for the assessment of pulmonary nodules. Thirty-six patients with 38 known or suspected malignant pulmonary nodules underwent PET scanning of the thorax at two time points: the first was at 70 minutes (range, 56 to 110) and the second was at 123 minutes (range, 100 to 163) after the intravenous administration of FDG. Tumor SUVs at the first and second time points were 3.66 ± 1.95 and 4.43 ± 2.43, respectively (ie, $20.5\% \pm 8.1\%$ increase between the two measurements; $P < .01$).

Four of 20 malignant tumors had SUVs of less than 2.5 on the first scan (range, 1.12 to 1.69). Benign lesions at the first and second time points had SUVs of 1.14 ± 0.64 and 1.11 ± 0.70, respectively (P value not significant). In this study, single-time point PET scanning with a threshold SUV of 2.5 (at time point 1) had a sensitivity of 80% and a specificity of 94%, while dual-time point scanning with a threshold value of a 10% increase in SUV between the first and second time points provided a sensitivity of 100% and a specificity of 89%.

Recent studies by Kumar and colleagues [26] and Mavi and colleagues [27] reported high sensitivity, specificity, and accuracy in breast carcinoma with a dual-time point approach. Kumar and colleagues studied 54 breast cancer patients with 57 breast lesions who underwent two sequential FDG-PET scans. The average percent change in the SUVs between time point 1 and time point 2 was calculated. All PET study results were correlated with follow-up surgical pathology results. Of the 57 breast lesions, 39 were invasive carcinoma and 18 were postbiopsy inflammation. Among the invasive carcinomas, 33 (85%) showed an increase and 6 (15%) showed either no change or a decrease in SUV over time. The percent change in SUVs in these tumors from time point 1 to time point 2 (mean ± SD) was +12.6% ± 11.4% (P = .003). Of the 18 inflammatory lesions, 3 (17%) showed an increase and 15 (83%) showed either no change or a decrease in SUVs. The percent change in SUVs from the time point 1 to the time point 2 (mean ± SD) was −10.2% ± 16.5% (P = .03). Of the 57 normal contralateral breasts, 2 (3.5%) showed an increase and 55 (96.5%) showed either no change or a decrease in SUVs. The percent change in SUVs from time point 1 to time point 2 (mean ± SD) was −15.8% ± 17% (P = .005). In the study by Mavi and colleagues [27], 152 patients with newly diagnosed breast cancer underwent two sequential PET scans for preoperative staging, and SUV_{max} was measured at both time points. The percent change in SUV_{max} (ΔSUV_{max}%) between time points 1 (SUV_{max1}) and 2 (SUV_{max2}) was calculated. Patients were divided into two groups according to histopathology as invasive and noninvasive. Invasive tumors were also divided into two groups (>10 mm and 4 to 10 mm). The tumor-to-contralateral normal breast (background) ratios of SUV_{max} at both time points for these two groups were measured and $\Delta\%SUV_{max}$ values were calculated. The mean ± SD of the SUV_{max1}, the SUV_{max2}, and the $\Delta\%SUV_{max}$ were 3.9 ± 3.7, 4.3 ± 4.0, and 8.3% ± 11.5% for invasive; 2.0 ± 0.6, 2.1 ± 0.6, and 3.4% ± 13.0% for noninvasive; and 1.2 ± 0.3, 1.1 ± 0.2, and −10.0% ± 10.8% for the contralateral normal breast groups, respectively. When SUV_{max1}, $\Delta\%SUV_{max}$, and the tumor-to-background ratios were compared among groups, all results were found to be significant ($P < .001$). They concluded that dual-time point imaging is a simple and noninvasive method that may improve the sensitivity and accuracy of FDG-PET in assessing patients with primary breast cancer. Lesion detectability increased from 83% at 1.5-hour images to 93% at 3-hour images in a study by Boerner and colleagues [25] in breast carcinoma.

Ma and colleagues [29] examined the usefulness of this technique in detecting para-aortic lymph node (PALN) metastases from cervical cancer. These data revealed that an additional scan at 3 hours is helpful for detecting PALN, especially for lower PALN metastases. Nishiyama and colleagues [28] investigated this approach in gallbladder carcinoma and concluded that delayed FDG-PET is more helpful than early FDG-PET for evaluating this cancer. Spence and colleagues [30] applied this method in supratentorial gliomas coupled with kinetic modeling. The estimated k_4 values for tumors were not significantly different from those of cerebral gray matter (GM) in early imaging but were lower at the delayed times. A report by Zhuang and colleagues [31] revealed an increase in SUV on delayed scans in known malignant lesions, whereas the SUVs of benign lung nodules decreased slightly over time. In contrast, the SUVs of the inflammatory lesions caused by radiation therapy and those of the lesions of painful lower limb prostheses remained stable over time. The application of this approach to predict the nature of the bone marrow FDG uptake was studied by Houseni and colleagues [32]. They noted that malignant lesions in the bone marrow result in significantly higher levels of FDG uptake over time than those affected by chemotherapeutic agents.

In many of these studies, the dual-time point approach improved both the sensitivity and the specificity of PET for various malignancies, including breast, lung, and head and neck cancers. This can be explained as follows: increasing FDG uptake over time in the malignant lesions allows differentiating them from benign etiologies with higher specificity, whereas increased lesion-to-background ratio (resulting from a combination of FDG washout from the surrounding normal tissues and enhanced FDG uptake in cancer) leads to higher sensitivity for detecting cancer. This is a noteworthy observation, as there is usually a trade-off between sensitivity and specificity for most other diagnostic tests when a new approach is adopted.

Future implications

In summary, several studies have demonstrated that absolute SUV measurement does not always allow for optimal separation of malignant from

benign lesions. Change in SUV over time may prove to be useful for improving the accuracy of FDG-PET imaging for this purpose. Delaying FDG-PET imaging beyond the traditional 1-hour time should also be considered since most lesions show increasing FDG uptake over the time up to several hours. When comparing lesions and in the same lesions noted on images, the SUV should be measured at the same time point to enhance its reliability.

Correction of standardized uptake value for the partial volume effect

The partial volume effect (PVE) is an important factor for measuring the radiotracer concentration with accuracy. This is mostly related to the scanner resolution and is applicable to objects with sizes less than 2 to 3 times the spatial resolution of the PET scanner. In addition, physiological and patient motions during data acquisition are also major factors in degrading spatial resolution, thereby also contributing to the PVE. The phenomenon is akin to what is observed with other imaging techniques including SPECT and structural imaging. Although extensively addressed in brain PET studies [33–39], this is a major source of concern in optimal assessment of malignant lesions [40]. Typically, the best resolution (as measured by laboratory experiments) achieved by the modern generation of clinical whole-body PET scanners is at best 4 mm (see the article by Zaidi and Alavi elsewhere in this issue). However, in clinical practice the actual spatial resolution of the reconstructed images is substantially less than that specified by phantom experiments owing to the limited statistics in the acquired data sets and the limitations of the reconstruction algorithms. This limited spatial resolution does not allow for an accurate measurement of the true SUV in structures and lesions less than 2 to 3 times the spatial resolution of the PET scanner as defined by the full-width at half-maximum (FWHM) of a point spread function. It is well known that the contrast between the lesion and the surrounding background decreases as the size of the lesion becomes smaller, and may disappear completely beyond a certain point [41]. Several approaches to minimize PVE have been described. Broadly, they can be categorized into three groups based on the following underlying principles (as seen in the article by Rousset and colleagues elsewhere in this issue): (1) methods that correct for resolution losses after reconstruction of images using various models, (2) methods that incorporate PVE modeling within the reconstruction process, and (3) methods that use the size of the lesion as determined by anatomic imaging data (eg, CT/MR imaging) to correct for PVE. We shall describe the latter approach in more detail since it is relevant and practical in the clinical settings.

With partial volume correction, Hickeson and colleagues [42] investigated this effect in the assessment of pulmonary lesions, and noted that there is a significant underestimation of SUV in lesions smaller than 2 cm in size. By correcting the measured value by using lesion size measured from the CT scan (which was assumed to represent the true size of the lesion), improved differentiation between malignant and benign lesions was achieved.

Hickeson and colleagues [42] reported an increase in accuracy from 58% to 89% in the metabolic activity of lung nodules measuring less than 2 cm when an SUV threshold of 2.5 was adopted to distinguish between benign and malignant lesions (Figs. 2–4). In this study, each lesion's SUV was determined by using two different methods. The maximum voxel SUV was determined in a circular ROI with a diameter of 0.8 cm (two voxels) at the plane with maximal FDG uptake in the lesion. In the second method, the SUV was corrected for underestimation of the true metabolic activity of the entire lesion because of the suboptimal spatial resolution and the PVE. Two ROIs were drawn around the lesion. The smaller of the two included all voxels associated with the lesion. In practice, this was drawn at least 0.8 cm outside the 50% uptake level of the maximum activity to include all of the counts resulting from the solitary pulmonary nodule. The second larger ROI surrounded the smaller ROI as well as its surrounding background. Thus, lesion background could be determined from the average uptake outside the smaller ROI and inside the larger ROI. Note that the halfway point between the maximum lesion activity and the surrounding background activity is frequently used as the true size of the lesion. The background uptake was then subtracted from the average uptake in the small ROI. Therefore, the corrected SUV was calculated by including the injected dose, the patient's weight, and time after injection by using the following formula:

$$corSUV = \frac{\frac{region's\ activity\ \ (MBq) - background\ activity\ \ (MBq)}{lesion's\ size\ on\ CT\ scan\ \ (cm^3)}}{\frac{Injected\ dose\ (MBq)}{Body\ weight\ (g)}} \quad (4)$$

Avril and colleagues [19] examined the role of a similar approach in breast cancer, and noted that correction of SUV for the PVE and normalization for blood glucose level yielded the highest diagnostic accuracy among several PET quantitative procedures. Lubberink and colleagues [43] compared the results of ^{110m}In-DTPA-D-Phe^1-octreotide PET images with those of the ^{111}In-DTPA-D-Phe^1-octreotide SPECT scans, and observed that partial volume correction greatly improved detection of small tumors and

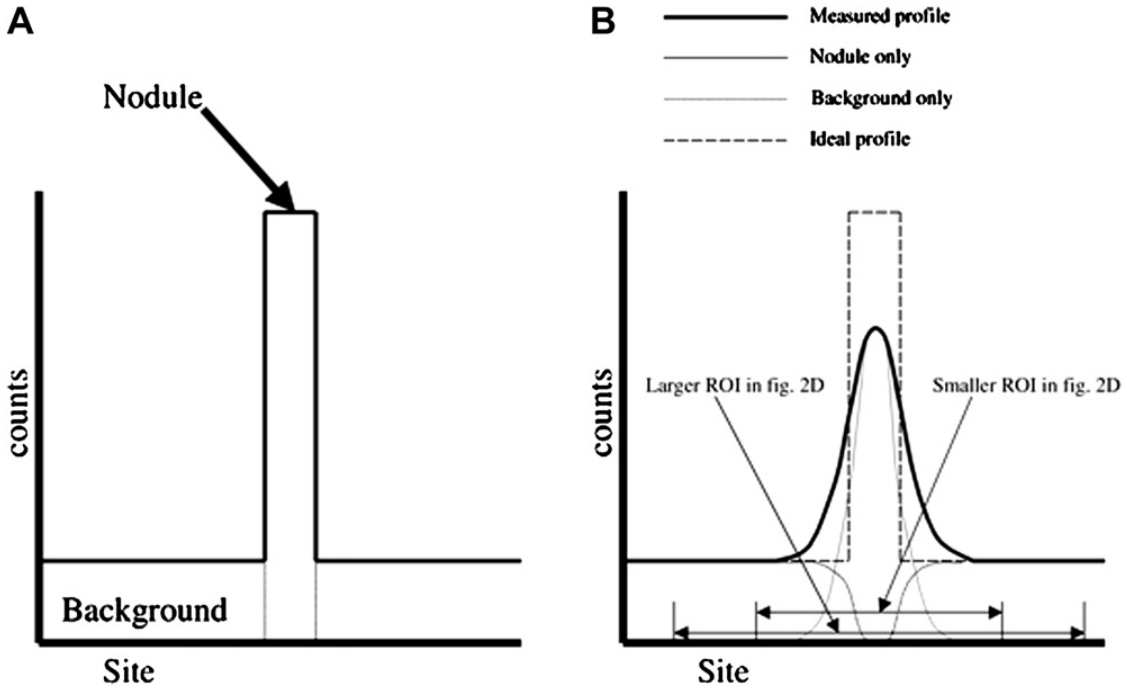

Fig. 2. (*A*) Profile of small lung nodule with uniform FDG uptake using "ideal" PET scanner with perfect spatial resolution; lung itself shows uniformly low FDG activity. (*B*) Profile of perceived FDG activity with current PET scanner through same nodule in same lung is indicated by thick-lined curve. True distribution of FDG (ideal profile) is indicated by broken line. Thin line indicates profile of perceived FDG activity from lung nodule and thinner line indicates that from uninvolved adjacent lung parenchyma (background). Note that area under profile using "ideal" PET scanner indicated in *A* is equal to that using current PET scanner indicated in *B*. (*Reprinted from* Hickeson M, Yun M, Matthies A, et al. Use of a corrected standardized uptake value based on the lesion size on CT permits accurate characterization of lung nodules on FDG-PET. Eur J Nucl Med Mol Imaging 2002; 29:1639–47; with kind permission from Springer Science and Business Media.)

allowed accurate quantitation of tracer concentration in lesions of various sizes (Fig. 5). From these studies, it is clear that PVE correction is crucial in the measurement of tumor FDG uptake in the small lesions. It is of importance when monitoring response to therapeutic intervention, where the reduction in the size of a tumor could result in underestimation of the true concentration of compounds such as FDG in the intended sites.

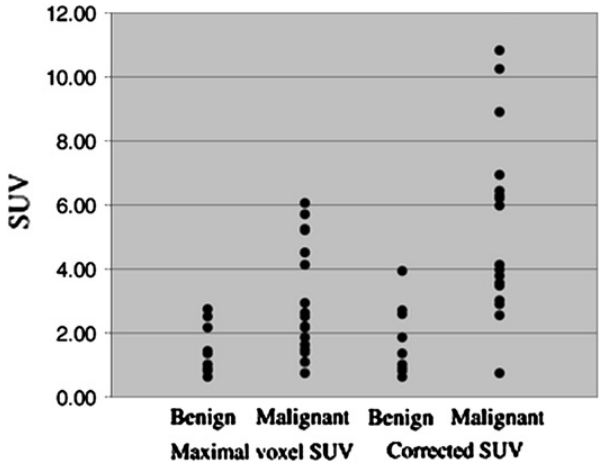

Fig. 3. SUVs of benign and malignant lung lesions measuring equal to or less than 2 cm using both methods. (*Reprinted from* Hickeson M, Yun M, Matthies A, et al. Use of a corrected standardized uptake value based on the lesion size on CT permits accurate characterization of lung nodules on FDG-PET. Eur J Nucl Med Mol Imaging 2002;29:1639–47; with kind permission from Springer Science and Business Media.)

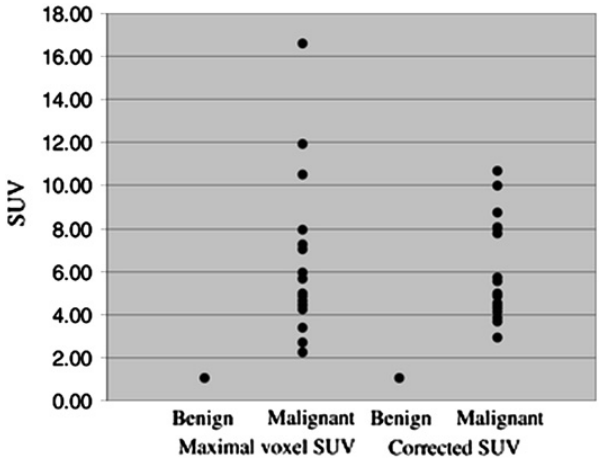

Fig. 4. SUVs of benign and malignant lung lesions measuring more than 2 cm using both methods. (*Reprinted from* Hickeson M, Yun M, Matthies A, et al. Use of a corrected standardized uptake value based on the lesion size on CT permits accurate characterization of lung nodules on FDG-PET. Eur J Nucl Med Mol Imaging 2002;29:1639–47; with kind permission from Springer Science and Business Media.)

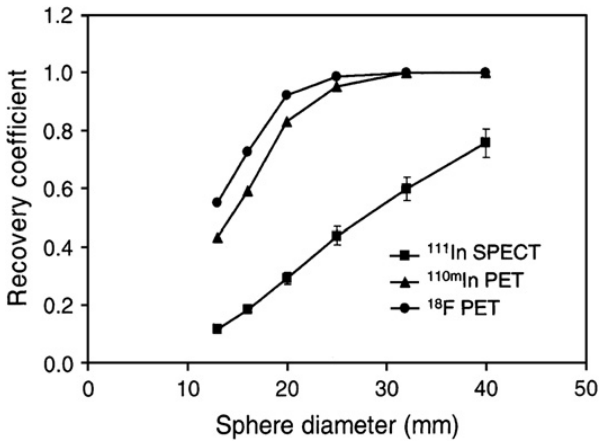

Fig. 5. Sphere recovery functions for partial volume correction for ^{110m}In-PET, ^{111}In-SPECT, and ^{18}F FDG-PET. (*Reprinted from* Lubberink M, Tolmachev V, Widstrom C, et al. 110mIn-DTPA-D-Phe1-octreotide for imaging of neuroendocrine tumors with PET. J Nucl Med 2002;43:1391–7; with permission of the Society of Nuclear Medicine.)

Applications of partial volume effect correction in neurology

Correction for partial volume correction was studied by investigators at the University of Pennsylvania in the 1980s when CT and low-resolution PET instruments were used to examine patients with Alzheimer's disease (AD) and other central nervous system disorders that usually result in cerebral atrophy [33]. This technique was later investigated by using modern segmentation methodologies and high-resolution MR imaging [44,45]. The latter has allowed for accurate measurement of GM and white matter (WM) as well as cerebrospinal fluid (CSF) volumes in the brain [46,47].

Kohn and colleagues [46] described a new computerized system developed to process standard spin-echo magnetic resonance imaging data for estimation of brain parenchyma and cerebrospinal fluid volumes. In phantom experiments, these estimated volumes corresponded closely to the true volumes ($r = 0.998$), with a mean error less than 1.0 cm^3 (for phantom volumes ranging from 5 to 35 cm^3), with excellent intra- and interobserver reliability. In a clinical validation study with actual brain images of 10 human subjects, the average coefficient of variation among observers for the measurement of absolute brain and CSF volumes was 1.2% and 6.4%, respectively. The intraclass correlation for three expert operators was found to be greater than 0.99 in the measurement of brain and ventricular volumes and greater than 0.94 for total CSF volume. The authors concluded that their technique to analyze MR images of the brain performed with acceptable levels of accuracy, and concluded that it can be used to measure brain and CSF volumes for clinical research. This technique, they believed, could be helpful in the correlation of neuroanatomic measurements to behavioral and physiological parameters in neuropsychiatric disorders.

Tanna and colleagues [34] adopted this computerized segmentation technique in a retrospective analysis of digitized T2-weighted MR images of 16 healthy elderly control subjects and 16 patients with AD. They quantified ventricular and extraventricular CSF and studied the effects of aging and AD on brain function as determined by FDG-PET. In both groups, the degree of atrophy as measured by these techniques was used to correct for metabolic rates obtained by PET. Patients with AD had higher total, extraventricular, total ventricular, and third ventricular CSF volumes (49%, 37%, 99%, and 74%, respectively), and 7% lower brain volumes than the control group. Patients with AD also showed a more marked decline in brain volumes and a greater increase in CSF volumes with advancing age than the control group. The patient group had a 25.0% increase in corrected whole-brain metabolic rates compared with the control group that had only a 15.8% increase by applying the partial volume correction factors. The use of this technique, they concluded, could provide a basis for further studies of aging and dementia, by calculating the accurate rates of regional metabolism of structural components in these settings.

Bural and colleagues [48] studied the effects of a novel quantitative MR imaging segmentation scheme that allows for actual SUV (instead of metabolic rates as reported by Tanna and colleagues [34] as referenced above) calculation of the regional GM, WM, and CSF volumes. This approach resulted in overcoming the difficulties associated with conventional low-resolution imaging techniques for measuring actual metabolic activity of the GM. These investigators calculated the volumes of GM, WM, and CSF by using a special segmentation technique on the MR images. This was followed by computation of the mean SUV representing the whole metabolic activity of the brain from the FDG-PET images. They also measured the WM SUV from the upper transaxial slices (centrum semiovale) of the FDG-PET images. The volumes of the GM, WM, and CSF were summed to calculate whole-brain volume to enable calculation of global cerebral metabolic activity by multiplying the mean SUV by the total-brain volume. Similarly, the whole-brain WM metabolic activity was measured by multiplying the mean SUV for the WM by the WM volume. CSF metabolic activity was considered to be 0. Thus, by subtracting the global WM metabolic activity from that of the whole brain, they were able to measure the global GM metabolic

activity alone. Finally, by dividing GM global metabolic activity by GM volume, an accurate SUV for GM alone was determined. The brain volumes ranged between 1100 and 1546 cm^3. The mean SUV for total brain was 4.8 to 7.0. Global cerebral metabolic activity of the brain ranged from 5565 to 9566 SUV cm^3. The mean SUV for WM was 2.8 to 4.1. Based on these measurements, they reported that the GM SUV in the sample examined ranged from 8.7 to 11.3.

Concept of global metabolic activity based on combined structure-function assessment in healthy and diseased states

The concept, methods, and the use of global metabolic activity have been described in the article by Basu and colleagues elsewhere in this issue. In this article, we shall briefly outline the principle of this method and its potentials. This approach was first used in assessment of the brain in patients with AD and in age-matched controls [49]. The method includes calculating tissue volume by using modern computer-based algorithms and accurate (partial volume corrected) measurement of metabolic activities (or other functional process) at each site of interest. The power of this approach is assessment of global disease activity in the patients, which certainly has several advantages over measuring SUV_{max} in one index lesion. This concept is particularly applicable to cancer both at the initial stage and following treatment to estimate the metabolic burden of the disease. This approach may prove to be essential for testing new therapeutic agents. Similarly, this approach can be effectively used in other states such as atherosclerosis [50], cancer, and cardiac disorders.

Summary

Quantitative PET imaging is superior to other modalities in many clinical and research applications. With the increasing role of FDG-PET in the field of oncology, reliable indices characterizing tumor activity is of immense importance for monitoring response to therapy [51]. Currently employed quantitative imaging with PET will undertake constant refinements for improving its impact in patient management. Sophisticated quantitative analysis methodologies are likely to become widely available in clinical settings and not just limited to PET research facilities with advanced scientific and technical support. This will enormously enhance the potential of FDG-PET to "personalize" treatment by evaluating the effectiveness of therapy and to recognize ineffective treatments that may also be costly or risky. Thus further refinements might prove invaluable for the optimal use of this powerful imaging technology.

Acknowledgments

This work was supported in part by the International Union against Cancer (UICC), Geneva, Switzerland, under the ACSBI fellowship and by Grant No. SNSF 3100A0-116547 from the Swiss National Foundation.

References

[1] Alavi A, Reivich M, Greenberg J, et al. Mapping of functional activity in brain with 18F-fluoro-deoxyglucose. Semin Nucl Med 1981;11:24–31.
[2] Reivich M, Alavi A, Wolf A, et al. Use of 2-deoxy-D[1-11C]glucose for the determination of local cerebral glucose metabolism in humans: variation within and between subjects. J Cereb Blood Flow Metab 1982;2:307–19.
[3] Zaidi H. Quantitative analysis in nuclear medicine imaging. New York: Springer; 2006.
[4] Sokoloff L, Reivich M, Kennedy C, et al. The [^{14}C]deoxyglucose method for the measurement of local cerebral glucose utilization: theory, procedure, and normal values in the conscious and anesthetized albino rat. J Neurochem 1977;28: 897–916.
[5] Reivich M, Kuhl D, Wolf A, et al. The [18F]fluorodeoxyglucose method for the measurement of local cerebral glucose utilization in man. Circ Res 1979;44:127–37.
[6] Phelps ME, Huang SC, Hoffman EJ, et al. Tomographic measurement of local cerebral glucose metabolic rate in humans with (F-18)2-fluoro-2-deoxy-D-glucose: validation of method. Ann Neurol 1979;6:371–88.
[7] Gjedde A. Calculation of cerebral glucose phosphorylation from brain uptake of glucose analogs in vivo: a re-examination. Brain Res Rev 1982;4:237–74.
[8] Patlak CS, Blasberg RG, Fenstermacher JD. Graphical evaluation of blood-to-brain transfer constants from multiple-time uptake data. J Cereb Blood Flow Metab 1983;3:1–7.
[9] Carson R. Tracer kinetic modeling in PET. In: Valk PE, Bailey DL, Townsend DW, et al, editors. Positron emission tomography: basic science and clinical practice. Chapter 4 edition. London: Springer-Verlag; 2003. p. 147–79.
[10] Hunter G, Hamberg L, Alpert N, et al. Simplified measurement of deoxyglucose utilization rate. J Nucl Med 1996;37:950–5.
[11] Huang S-C. Anatomy of SUV. Nucl Med Biol 2000;27:643–6.
[12] Minn H, Leskinen-Kallio S, Lindholm P, et al. [18F]fluorodeoxyglucose uptake in tumors: kinetic vs. steady-state methods with reference to plasma insulin. J Comput Assist Tomogr 1993; 17:115–23.

[13] Kole A, Nieweg O, Pruim J, et al. Standardized uptake value and quantification of metabolism for breast cancer imagin with FDG and L-[1-11C] tyrosine PET. J Nuc Med 1997;38:692–6.
[14] Keyes J. SUV: standard uptake value or silly useless value? J Nucl Med 1995;36:1836–9.
[15] Kim CK, Gupta N, Chandramouli B, et al. Stardized uptake values of FDG: body surface area correction is preferable to body weight correction. J Nucl Med 1994;35:164–7.
[16] Kim CK, Gupta N. Dependency of standardized uptake values of fluorine-18 fluorodeoxyglucose on body size: comparison of body surface area correction and lean body mass correction. Nucl Med Commun 1996;17:890–4.
[17] Gupta N, Frank A, Dewan N, et al. Solitary pulmonary nodules: detection of malignancy with PET with 2-[F-18]-fluoro-2-deoxy-D-glucose. Radiology 1992;184:441–4.
[18] Zasadny KR, Wahl RL. Standardized uptake values of normal tissues at PET with 2-[fluorine-18]-fluoro-2-deoxy-D-glucose: variations with body weight and a method for correction. Radiology 1993;189:847–50.
[19] Avril N, Bense S, Ziegler SI, et al. Breast imaging with fluorine-18-FDG PET: quantitative image analysis. J Nucl Med 1997;38:1186–91.
[20] Zhuang HM, Cortes-Blanco A, Pourdehnad M, et al. Do high glucose levels have differential effect on FDG uptake in inflammatory and malignant disorders? Nucl Med Commun 2001;22: 1123–8.
[21] Hamberg LM, Hunter GJ, Alpert NM, et al. The dose uptake ratio as an index of glucose metabolism: useful parameter or oversimplification? J Nucl Med 1994;35:1308–12.
[22] Lodge M, Lucas J, Marsden P, et al. A PET study of (18)FDG uptake in soft tissue masses. Eur J Nucl Med 1999;26:22–30.
[23] Hustinx R, Smith RJ, Benard F, et al. Dual time point fluorine-18 fluorodeoxyglucose positron emission tomography: a potential method to differentiate malignancy from inflammation and normal tissue in the head and neck. Eur J Nucl Med 1999;26:1345–8.
[24] Matthies A, Hickeson M, Cuchiara A, et al. Dual time point 18F-FDG PET for the evaluation of pulmonary nodules. J Nucl Med 2002;43:871–5.
[25] Boerner AR, Weckesser M, Herzog H, et al. Optimal scan time for fluorine-18 fluorodeoxyglucose positron emission tomography in breast cancer. Eur J Nucl Med 1999;26:226–30.
[26] Kumar R, Loving VA, Chauhan A, et al. Potential of dual-time-point imaging to improve breast cancer diagnosis with 18F-FDG PET. J Nucl Med 2005;46:1819–24.
[27] Mavi A, Urhan M, Yu JQ, et al. Dual time point 18F-FDG PET imaging detects breast cancer with high sensitivity and correlates well with histologic subtypes. J Nucl Med 2006;47:1440–6.
[28] Nishiyama Y, Yamamoto Y, Fukunaga K, et al. Dual-time-point 18F-FDG PET for the evaluation of gallbladder carcinoma. J Nucl Med 2006;47: 633–8.
[29] Ma SY, See LC, Lai CH, et al. Delayed (18)F-FDG PET for detection of paraaortic lymph node metastases in cervical cancer patients. J Nucl Med 2003;44:1775–83.
[30] Spence AM, Muzi M, Mankoff DA, et al. 18F-FDG PET of gliomas at delayed intervals: improved distinction between tumor and normal gray matter. J Nucl Med 2004;45:1653–9.
[31] Zhuang H, Pourdehnad M, Lambright ES, et al. Dual time point 18F-FDG PET imaging for differentiating malignant from inflammatory processes. J Nucl Med 2001;42:1412–7.
[32] Houseni M, Chamroonrat W, Bural G, et al. Promising role of dual time FDG-PET imaging in assessing focal and diffuse bone marrow disorders. J Nuc Med 2006;47:227P.
[33] Chawluk J, Alavi A, Dann R, et al. Positron emission tomography in aging and dementia: effect of cerebral atrophy. J Nucl Med 1987;28: 431–7.
[34] Tanna NK, Kohn MI, Horwich DN, et al. Analysis of brain and cerebrospinal fluid volumes with MR imaging: impact on PET data correction for atrophy. Part II. Aging and Alzheimer dementia. Radiology 1991;178:123–30.
[35] Rousset OG, Ma Y, Evans AC. Correction for partial volume effects in PET: principle and validation. J Nucl Med 1998;39:904–11.
[36] Aston JA, Cunningham VJ, Asselin MC, et al. Positron emission tomography partial volume correction: estimation and algorithms. J Cereb Blood Flow Metab 2002;22:1019–34.
[37] Quarantelli M, Berkouk K, Prinster A, et al. Integrated software for the analysis of brain PET/SPECT studies with partial-volume-effect correction. J Nucl Med 2004;45:192–201.
[38] Baete K, Nuyts J, Van Laere K, et al. Evaluation of anatomy based reconstruction for partial volume correction in brain FDG-PET. NeuroImage 2004; 23:305–17.
[39] Zaidi H, Ruest T, Schoenahl F, et al. Comparative evaluation of statistical brain MR image segmentation algorithms and their impact on partial volume effect correction in PET. Neuroimage 2006;32:1591–607.
[40] Soret M, Bacharach SL, Buvat I. Partial-volume effect in PET tumor imaging. J Nucl Med 2007; 48:932–45.
[41] Weber W, Young C, Abdel-Dayem HM, et al. Assessment of pulmonary lesions with 18F-fluorodeoxyglucose positron imaging using coincidence mode gamma cameras. J Nucl Med 1999; 40:574–8.
[42] Hickeson M, Yun M, Matthies A, et al. Use of a corrected standardized uptake value based on the lesion size on CT permits accurate characterization of lung nodules on FDG-PET. Eur J Nucl Med Mol Imaging 2002;29:1639–47.
[43] Lubberink M, Tolmachev V, Widstrom C, et al. 110mIn-DTPA-D-Phe1-octreotide for imaging of

neuroendocrine tumors with PET. J Nucl Med 2002;43:1391–7.
[44] Muller-Gartner HW, Links JM, Prince JL, et al. Measurement of radiotracer concentration in brain gray matter using positron emission tomography: MRI-based correction for partial volume effects. J Cereb Blood Flow Metab 1992;12: 571–83.
[45] Meltzer CC, Zubieta JK, Links JM, et al. MR-based correction of brain PET measurements for heterogeneous gray matter radioactivity distribution. J Cereb Blood Flow Metab 1996;16:650–8.
[46] Kohn MI, Tanna NK, Herman GT, et al. Analysis of brain and cerebrospinal fluid volumes with MR imaging. Part I. Methods, reliability, and validation. Radiology 1991;178:115–22.
[47] Zhuge Y, Liu J, Udupa JK. Membership-based multiprotocol MR brain image segmentation. Medical Imaging 2003: Image Processing. San Diego (CA), USA, 2003/05/16/, 5032:1572–9.
[48] Bural GG, Zhuge Y, Torigian DA, et al. Partial volume correction and segmentation allows accurate measurement of SUV for the grey matter in the brain. J Nuc Med 2006;47:9P.
[49] Alavi A, Newberg AB, Souder E, et al. Quantitative analysis of PET and MRI data in normal aging and Alzheimer's disease: atrophy weighted total brain metabolism and absolute whole brain metabolism as reliable discriminators. J Nucl Med 1993;34:1681–7.
[50] Bural GG, Torigian DA, Chamroonrat W, et al. Quantitative assessment of the atherosclerotic burden of the aorta by combined FDG-PET and CT image analysis: a new concept. Nucl Med Biol 2006;33:1037–43.
[51] Basu S, Alavi A. Defining co-related parameters between 'metabolic' flare and 'clinical', 'biochemical', and 'osteoblastic' flare and establishing guidelines for assessing response to treatment in cancer. Eur J Nucl Med Mol Imaging 2006;34:441–3.